OVERVIEW OF MAGNETIC SUSPENSION RESEARCH AT LANGLEY RESEARCH CENTER

Nelson J. Groom

SUMMARY

An overview of research in small- and large-gap magnetic suspension systems at Langley Research Center (LaRC) is presented. The overview is limited to systems which have been built as laboratory models or engineering models. Small-gap systems applications include the Annular Momentum Control Device (AMCD), which is a momentum storage device for the stabilization and control of spacecraft, and the Annular Suspension and Pointing System (ASPS), which is a general purpose pointing mount designed to provide orientation, mechanical isolation, and fine pointing of space experiments. These devices are described and control and linearization approaches for the magnetic suspension systems for these devices are discussed. Large-gap systems applications at LaRC have been almost exclusively wind tunnel magnetic suspension systems. A brief description of these efforts is also presented.

INTRODUCTION

Research in small-gap magnetic suspension systems at Langley Research Center (LaRC) began in the early 1970's with the development of the Annular Momentum Control Device (AMCD) concept. The AMCD is a momentum storage device with applications to the stabilization and control of spacecraft (ref. 1). This research was continued with the development of the Annular Suspension and Pointing System (ASPS) concept. The ASPS is a derivative of the AMCD and is a general purpose pointing mount designed to provide orientation, mechanical isolation, and fine pointing of space experiments (refs. 2 and 3). These devices will be described, and control and linearization approaches for the magnetic suspension systems for these devices will be discussed.

Research in large-gap magnetic suspension systems at LaRC began in the early 1960's and has been focused almost entirely on wind tunnel systems. The research began with the development of a single degree-of-freedom demonstration system (ref. 4) and has continued to the present with design studies of large-scale systems with superconducting magnets (ref. 5). A brief description of the wind tunnel magnetic suspension system efforts at LaRC will be presented.

SMALL-GAP SUSPENSION SYSTEMS

Annular Momentum Control Device (AMCD)

Magnetic suspension has historically been viewed as a promising solution to several problems encountered in the long-term utilization of momentum storage devices for spacecraft control. However, earlier efforts toward the application of magnetic suspension technology were focused on developing a direct physical replacement for the mechanical bearings of conventional shaft-driven and suspended-steel flywheels. The conventional approach, using a central hub with a shaft to provide support for both translational forces and rotational moments, was motivated in part by the need to keep the bearings self-contained and as small as possible so that bearing surface speed and drag effects could be kept to acceptable levels. With magnetic suspension there are no contacting surfaces and, with proper design,

drag losses can be made relatively small. Therefore, bearing surface speed ceases to be a constraint. A reexamination of conventional approaches to the design of momentum storage devices on both a device and system level, without the bearing surface speed constraint, led to the concept of the AMCD (ref. 6). The basic concept of the AMCD consists of a spinning annular rim suspended by a minimum of three noncontacting magnetic suspension stations and is driven by a noncontacting electromagnetic spin motor. The use of a thin annular rim provides the maximum momentum-to-mass ratio for any material since the spinning mass is concentrated at the largest mean radius. Significant improvements in this ratio can be obtained by using lightweight, high strength, composite materials since, for a rim, the stresses due to rotation are predominantly circumferential. The utilization of noncontacting suspension and driving elements eliminates mechanical wear and lubrication subsystem failures and results in system reliability characteristics equal to those of the magnetic suspension and rim drive motor electronics. A further advantage of the magnetic suspension system is that it can be tuned to provide for effective isolation of vibrations, generated by the rotating rim, from the vehicle and its scientific payloads. In addition, the magnetic suspension can produce smooth forces without threshold type nonlinearities (i.e., no mechanical breakout forces). The advantage of this characteristic is that small, precision, precessional torques can be generated by "gimbaling" the rim in the magnetic gaps.

In order to investigate technology requirements and evaluate certain design approaches, the AMCD was implemented as a laboratory test model. The laboratory model, shown in figure 1, consists of a graphite/epoxy composite rim, three magnetic suspension stations, three spin motor stator element pairs (one pair per suspension station), and six pneumatic backup bearings (required for laboratory use only). The suspension assemblies are attached to an aluminum base plate. A vacuum cover fits over the suspension-motor-rim-backup bearing assembly and bolts to the base plate for high-speed spin tests. The rim is 1.7m (5.5 ft) in diameter, weighs 22.68 kg (50 lb), and is designed to rotate at 2,741 rpm. The rim momentum at this speed is 4,068 N-m-s (3,000 ft-lb-sec). A detailed description of the AMCD laboratory test model, as delivered, is given in reference 7, and preliminary test results are presented in reference 8. Additional information related to the laboratory model is available in references 9–16. Potential applications of the AMCD concept are presented in references 17–22.

Annular Suspension and Pointing System (ASPS)

The ASPS was developed to meet the need for a multipurpose experiment pointing platform which was established during NASA Earth-orbital systems technology guidance and control planning activities in the early 1970's. The ASPS is a derivative of the AMCD and uses a similar magnetic bearing design and suspension technique. However, the two are very different in purpose and operation (refs. 23–24). The ASPS (fig. 2) consists of a vernier assembly, which uses magnetic suspension, and a mechanical gimbal assembly, which uses conventional *dc* motor technology. The magnetic suspension of the vernier assembly provides high accuracy pointing (0.01 arcsec) and isolation from carrier motion disturbances. The mechanical gimbal assembly allows for system deployment, target acquisition and tracking, retargeting, and can serve as a backup, at reduced performance levels, in case of vernier assembly failure. A typical payload-ASPS-carrier vehicle configuration is shown in figure 3.

In order to demonstrate the very high accuracy pointing and control capability of the ASPS concept, a decision was made to fabricate and test an engineering model of the ASPS. The ASPS vernier assembly engineering model, with payload plate removed, is shown in figure 4. The payload plate bolts to the annular rotor which is suspended by five magnetic bearing actuators (MBA's) that provide control over three translational axes and rotations about the two transverse axes. Control about the roll axis is provided by a segmented *ac* induction motor. Power and data to and from the payload are provided by a rotary transformer and an optical coupler, respectively. Therefore, the only connection between payload and carrier vehicle is through the stiffness of the MBA servo loops which, because of the decoupling scheme used (ref. 2), acts through the payload's center of mass.

Additional information on the ASPS design and development and related analyses and simulations are presented in references 25–31.

SMALL-GAP ACTUATOR LINEARIZATION AND CONTROL APPROACHES

In order to define the basic type of small-gap magnetic bearing actuator which will be discussed in this paper, the simplified schematic of figure 5 is introduced. Shown are upper and lower electromagnets with currents I_U and I_L, producing forces F_U and F_L on a suspended element positioned in the center between the electromagnets at a gap distance G_o from the top electromagnet pole face. Since an electromagnet of the type being discussed produces an attractive force only, two are required to produce a bidirectional force capability. A position sensor is shown which measures the displacement G_s of the suspended element with respect to the centered position G_o. Position information is required for active control of the suspended element and is also required for some of the linearization approaches to be discussed. Under ideal assumptions, the force produced by a given electromagnet is directly proportional to the square of the coil current and inversely proportional to the square of the electromagnet gap (ref. 10) and can be written as

$$F = K(I^2/G^2) \tag{1}$$

Two approaches have been investigated for controlling this type of actuator. One approach involves controlling the upper and lower electromagnets differentially about a bias flux. The bias flux can either be supplied by permanent magnets in the magnetic circuit or by bias currents. In the other approach, either the upper electromagnet or the lower electromagnet is controlled depending on the direction of the force required.

Bias Flux Linearization and Control Approaches

Permanent Magnet.- The original control approach used for the laboratory model AMCD magnetic actuators was permanent magnet flux biasing. The operation of a permanent magnet flux-biased magnetic actuator can be described by referring to figure 6. This figure is a simplified schematic which shows a single actuator, for control along a single axis, which consists of a pair of magnetic bearing elements with permanent magnets mounted in the cores. The bearing elements are shown connected in a differential configuration. That is, for

a given input, the amplifier driver shown in the figure produces current in a direction to aid the permanent-magnet-produced flux in one element and, at the same time, produces equal current in a direction to subtract from the permanent-magnet-produced flux in the other element. This change in flux results in a net force produced on the suspended mass in a direction dependent on the polarity of the input to the amplifier driver. The force produced by this type actuator as a function of current, I, and gap, G, can be written as (from ref. 10)

$$F = \frac{K_1}{4}\left(\frac{[I_o + I]^2}{[x_o - G]^2} - \frac{[I_o - I]^2}{[x_o + G]^2}\right) \tag{2}$$

where K_1, $\bar{x}_o$, and I_o are constants (defined in ref. 10). I_o can be thought of as an equivalent constant bias current provided by the permanent magnets. Figure 7 shows the composite force-current characteristic of this type actuator with the suspended mass centered in the gaps. This figure illustrates a linear electromagnet gain of the actuator at a given gap position. By performing a first order linearization of equation 2 about a fixed operating point, the actuator force as a function of differential coil current and displacement can be written as

$$F = K_B I + K_M G \tag{3}$$

where K_B is an equivalent electromagnet gain and K_M is an equivalent bias flux stiffness (for more detail see ref. 10). These gains would be different for different operating points.

Variable Bias Current.- A variation of the permanent-magnet flux bias approach was developed for the ASPS in order to provide a linear actuator characteristic over a wide gap range. This approach uses variable bias currents to provide the bias flux. Figure 8 is a simplified block diagram of the variable bias current approach that was implemented for the ASPS. As can be seen by working through the block diagram, the bias current and control currents of the upper and lower electromagnets are adjusted so that the bias force produced by each and the net force produced by a given command force are equal regardless of the suspended mass's location in the gap. The unbalanced bias-flux stiffness is thus eliminated and the electromagnet gain is constant. A detailed description of this implementation is given in reference 25.

Flux Feedback.- When considering simplicity, efficiency, and controllability of force around zero, the permanent magnet flux bias approach trades off better than the other magnetic bearing control and linearization approaches that were discussed in the previous sections. Disadvantages of this approach include a minimum bandwidth requirement for stability (ref. 8) and linear operation over a restricted gap range about a fixed operating point. The variable bias current approach used in the ASPS suspension system was developed to overcome these disadvantages. However, since current is the controlled variable, the implementation of this approach is relatively complicated and requires actuator core material and rotor material with very low hysteresis in order to provide a sufficiently accurate force-output to force-command transfer characteristic (ref. 25). By using flux feedback (fig. 9), the complex current calculation, with the attendant requirement for gap compensation, is no longer required. In addition, the nonlinear transfer characteristic between electromagnet coil current and flux is included in the forward loop of a feedback system with very high open loop gain. This reduces the sensitivity of the force-output to force-input transfer characteristic to a negligible level as long as the actuator is operated below the saturation flux density of

the electromagnet core material and rotor material. Bias flux can be supplied by either fixed bias currents or permanent magnets in the flux feedback approach. In most applications, permanent magnet flux bias is the preferred approach because of power consumption and actuator heating issues.

The force produced by a given electromagnet, as a function of current and gap, is given by equation 1. Under the same assumptions, the force produced by a given electromagnet, as a function of flux in the electromagnet gap, can be written as (ref. 16)

$$F = K\phi^2 \tag{4}$$

where ϕ is flux and K is defined in reference 16. Using figure 5 and the associated nomenclature again, the force produced by the upper and lower elements becomes

$$F_U = K\phi_U^2, F_L = K\phi_L^2 \tag{5}$$

For a bearing element pair with differential control of flux, the total force becomes

$$F_T = K(\phi_U^2 - \phi_L^2) \tag{6}$$

With differential control about a bias flux, ϕ_o, the flux in the upper and lower gaps becomes

$$\phi_U = \phi_o + \phi_c, \ \phi_L = \phi_o - \phi_c \tag{7}$$

where ϕ_c is flux command. Substituting equation 7 into equation 6 results in

$$F_T = K([\phi_o^2 + 2\phi_o\phi_c + \phi_c^2] - [\phi_o^2 - 2\phi_o\phi_c + \phi_c^2]) \tag{8}$$

which simplifies to

$$F_T = 4K\phi_o\phi_c \tag{9}$$

By defining $\phi_c = F_c$ and $K_F = 4K\phi_o$, the total actuator force output, F_T, as a function of command force input, F_c, can be written as

$$F_T = K_F F_c \tag{10}$$

Single Element Linearization and Control Approaches

As mentioned above, single element control involves controlling either the upper or lower electromagnet (shown in fig. 5), depending on the direction of the force required. Controlling the electromagnets in this way results in a highly nonlinear force-current characteristic. This is illustrated by figure 10 which shows the composite force-current characteristic of a magnetic actuator with individual element control and with the suspended mass centered in the actuator gaps. It should be noted that this curve is based on ideal assumptions, and that in practice, because of hardware considerations, the smooth crossover at zero is difficult to achieve.

Two linearization approaches have been investigated for individual element control. One approach, which has been implemented for the laboratory model AMCD, utilizes the analog solution of the force equation for a given element. Figure 11 is a simplified block diagram of this implementation which uses analog multipliers and square root modules. The equations for upper and lower elements are included in the figure. A detailed description of this implementation is given in reference 12. This approach proved to be very sensitive to bearing element calibration and alignment accuracy.

The other linearization approach investigated for individual element control is microprocessor based and uses a table lookup to generate control signals. This approach was bench tested but has not been used in the AMCD laboratory model suspension system. Figure 12 is a block diagram representation of the laboratory implementation. In this approach, actual calibration data for a given bearing element pair are used to build a lookup table which is stored in the memory of a microprocessor system. Using the force command and gap position as input data, the correct value of current input to the coil, for the suspended element centered in the actuator gaps, is obtained by using a table lookup routine. This current is compensated for displacement from center by multiplying by the calculated gap. This approach is described in more detail and test results are presented in reference 15.

LARGE-GAP SYSTEMS

Interest in large-gap magnetic suspension systems at NASA Langley began in the early 1960's. The principal goal was the elimination of aerodynamic support interference in wind tunnel testing, which can cause significant corruption of wind tunnel results, as illustrated in figure 13. A single degree-of-freedom demonstration suspension system was operational in 1964 (ref. 4) and is shown in figure 14. The suspension coil was 16 inches in overall diameter, water cooled and split into two independent windings, and fed from a *dc* "bias" supply and a unipolar SCR power amplifier. Figure 15 is a schematic of the major circuit components.

For almost a decade, the principal LaRC MSBS activity was through grants and contracts with the Massachusetts Institute of Technology (MIT) and the University of Virginia (UVA). Information on these efforts is presented in references 32 and 33. An extensive list of related publications can be found in reference 34. MIT constructed two small-scale MSBSs and used them for a variety of testing at subsonic and supersonic speeds. The MIT 6-inch system was a relatively sophisticated and successful design and was eventually moved to LaRC in 1980. The system is now operated by the Instrument Research Division, principally to aid in the development of more accurate position sensors and force calibration techniques. A schematic diagram of the system is shown in figure 16. UVA also constructed two systems; the superconducting system is believed to be the first superconducting suspension system of any type. The system was decommissioned in the late 1970's and the electromagnet array is now kept at LaRC for historical interest.

LaRC also supported research at the University of Southampton from the late 1970's until recently (refs. 34–35). Notable achievements were the development of a digital control system, demonstration of roll control techniques (providing control of the sixth degree-of-freedom), and the construction of a superconducting model core (ref. 36) which is the small model shown in figure 17.

The LaRC 13-inch MSBS was originally constructed at AEDC, Tullahoma, TN and was transferred to LaRC in 1979. Since then, almost all the original hardware has been replaced, including the control system (now digital), position sensors, and main electromagnets. The system is installed in a low-speed wind tunnel, illustrated in figure 18, and has been used for extensive aerodynamic testing (refs. 37–38). For many years, this system was the largest air-gap suspension system known, but it has recently been surpassed by other wind tunnel systems in the U.S.S.R. and Japan.

Under various contracts with General Electric Company and Madison Magnetics Incorporated (MMI), a series of design studies of large-scale MSBSs were completed (ref. 5). MMI also designed and constructed a second-generation superconducting solenoid model core, which is the large model shown in figure 17.

CONCLUDING REMARKS

An overview of research in small- and large-gap magnetic suspension systems at Langley Research Center has been presented. The overview was limited to systems which have been built as laboratory models or engineering models. Small-gap systems applications have been focused on space applications and include advanced spacecraft control actuators and experiment isolation and pointing mounts. Large-gap systems applications have been almost exclusively wind tunnel magnetic suspension systems. A comprehensive list of references which provides more details on the systems discussed in the overview was also presented.

REFERENCES

1. Anderson, Willard W.; and Groom, Nelson J.: The Annular Momentum Control Device (AMCD) and Potential Applications. NASA TN D-7866, March 1975.
2. Anderson, Willard W.; and Joshi, Suresh M.: The Annular Suspension and Pointing (ASP) System for Space Experiments and Predicted Pointing Accuracies. NASA TR R-448, December 1975.
3. Anderson, Willard W.; Groom, Nelson J.; and Woolley, Charles T.: The Annular Suspension and Pointing System. Journal of Guidance and Control, Vol. 2, No. 5, September–October 1979, pp. 367–373.
4. Hamlet, Irving L.; and Kilgore, Robert A.: Some Aspects of an Air-Core Single-Coil Magnetic Suspension System. Presented at the ARL Symposium on Magnetic Wind Tunnel Suspension and Balance Systems. April 1966.
5. Boom, Roger W.; Abdelsalam, Mustafa K.; Eyssa, Y. M.; and McIntosh, G. E.: Magnetic Suspension and Balance System Advanced Study-Phase II. NASA CR-4327, November 1990.
6. Anderson, Willard W.; and Groom, Nelson J.: Annular Momentum Control Device. U.S. Letters Patent No. 3,915,416; October 28 1975.
7. Ball Brothers Research Corporation: Annular Momentum Control Device (AMCD). Volume I: Laboratory Model Development. NASA CR-144917, 1976.

8. Groom, Nelson J.; and Terray, David E.: Evaluation of a Laboratory Test Model Annular Momentum Control Device. NASA TP-1142, March 1978.

9. Groom, Nelson J.: Fixed-Base and Two-Body Equations of Motion for an Annular Momentum Control Device (AMCD). NASA TM-78644, March 1978.

10. Groom, Nelson J.: Analytical Model of An Annular Momentum Control Device (AMCD) Laboratory Test Model Magnetic Bearing Actuator. NASA TM-80099, August 1979.

11. Groom, Nelson J.; and Waldeck, Gary C.: Magnetic Suspension System for a Laboratory Model Annular Momentum Control Device. Presented at the AIAA Guidance and Control Conference, Boulder, Colorado, August 1979. (Available as AIAA Paper 79-1755).

12. Sperry Flight Systems: Magnetic Suspension System for an Annular Momentum Control Device (AMCD). NASA CR-159255, December 1979.

13. Woolley, Charles T.; and Groom, Nelson J.: Description of a Digital Computer Simulation of an Annular Momentum Control Device (AMCD) Laboratory Test Model. NASA TM-81797, 1981.

14. Groom, Nelson J.; Woolley, Charles T.; and Joshi, Suresh M.: Analysis and Simulation of a Magnetic Bearing Suspension System for a Laboratory Model Annular Momentum Control Device. NASA TP-1799, March 1981.

15. Groom, Nelson J.; and Miller, James B.: A Microprocessor—Based Table Lookup Approach for Magnetic Bearing Linearization. NASA TP-1838, 1981.

16. Groom, Nelson J.: A Magnetic Bearing Control Approach Using Flux Feedback. NASA TM-100672, March 1989.

17. Ball Brothers Research Corporation: Annular Momentum Control Device (AMCD). Volume II: Application To A Large Space Telescope. NASA CR-144917, 1976.

18. Nadkarni, Arun A.; and Joshi, Suresh M.: Optimal Maneuvering and Fine-Pointing Control of a Large Space Telescope with a New Magnetically Suspended, Single Gimbaled, Momentum Storage Device. Proceedings of the 15th IEEE Conference on Decision and Control, Clearwater Beach, FL, December 1–3, 1976.

19. Nadkarni, Arun A.; Groom, Nelson J.; and Joshi, Suresh M.: Optimal Fine Pointing of a Large Space Telescope using an Annular Momentum Control Device. Proceedings of the IEEE Southeastcon 77, Williamsburg, VA, April 4–6, 1978.

20. Joshi, Suresh M.; and Groom, Nelson J.: A Two-Level Controller Design Approach for Large Space Structures. Proceedings of the 1980 Joint Automatic Control Conference, San Francisco, CA, August 13–15, 1980.

21. Joshi, Suresh M.; and Groom, Nelson J.: Modal Damping Enhancement in Large Space Structures Using AMCD's. Journal of Guidance and Control, Vol. 3, No. 5, September–October 1980, pp. 477–479.

22. Joshi, Suresh M.: Damping Enhancement and Attitude Control of Large Space Structures. Proceedings of the 19th IEEE Conference on Decision and Control, Albuquerque, NM, December 10-12, 1980.

23. Anderson, Willard W.; and Groom, Nelson J.: Magnetic Suspension and Pointing System. U.S. Letters Patent No. 4,088,018, May 9, 1978.

24. Anderson, Willard W.; and Groom, Nelson J.: Magnetic Suspension and Pointing System. U.S. Letters Patent No. 4,156,548, May 29, 1979.

25. Cunningham, D. C.; Gismondi, T. P.; and Wilson, G. W.: System Design of the Annular Suspension and Pointing System (ASPS). Presented at the AIAA Guidance and Control Conference, Palo Alto, California, August 1978. (Available as AIAA Paper 78-1311).

26. Cunningham, David C.; et. al.: Design of the Annular Suspension and Pointing System (ASPS). NASA CR-3343, October, 1980.

27. Keckler, Claude R.; Kibler, Kemper S.; and Rowell, Larry F.: Determination of ASPS Performance for Large Payloads in the Shuttle Orbiter Disturbance Environment. NASA TM-80136, October, 1979.

28. Keckler, Claude R.: ASPS Performance with Large Payloads Onboard the Shuttle Orbiter. AIAA Journal of Guidance, Control, and Dynamics, Vol. 5, No. 1, pp. 32–36, January–February 1982.

29. Hamilton, Brian J.: Vibration Attenuation Using Magnetic Suspension Isolation. Presented at the Joint Automatic Control Conference, Charlottesville, VA, June 17–19, 1981.

30. Hamilton, Brian J.: Laboratory Evaluation of the Pointing Stability of the ASPS Vernier System. NASA CR-159307, June, 1980

31. Sperry Flight Systems: The Development of the ASPS Vernier System. Final Report under Contract No. NAS1-15008, June, 1983.

32. Covert, E. E.; Finston, M.; Vlajinac, M.; and Stephens, T.: Magnetic Balance and Suspension Systems for Use with Wind Tunnels. Progress in Aerospace Sciences, Volume 14, 1973.

33. Zapata, R. N.: Development of a Superconducting Electromagnetic Suspension and Balance System for Dynamic Stability Studies. NASA CR-132255, February 1973.

34. Tuttle, M. H.; Moore, D. L.; and Kilgore, R. A.: Magnetic Suspension and Balance Systems—A comprehensive, annotated, bibliography. NASA TM-4318, August 1991.

35. Britcher, C. P.: Progress toward Magnetic Suspension and Balance Systems for Large Wind Tunnels. AIAA Journal of Aircraft, Volume 22, April 1985.

36. Britcher, C. P.; Goodyer, M. J.; Scurlock, R. G.; and Wu, Y. Y.: A Flying Superconducting Model and Cryostat for Magnetic Suspension of Wind Tunnel Models. Cryogenics, April, 1984.

37. Dress, D. A.: Drag Measurements on a Laminar-Flow Body of Revolution in the 13-inch Magnetic Suspension and Balance System. NASA TP-2895, April, 1989.

38. Britcher, C. P.; and Alcorn, C. W.: Interference-Free Measurements of the Subsonic Aerodynamics of Slanted-Base Ogive Cylinders. AIAA Journal, April, 1991.

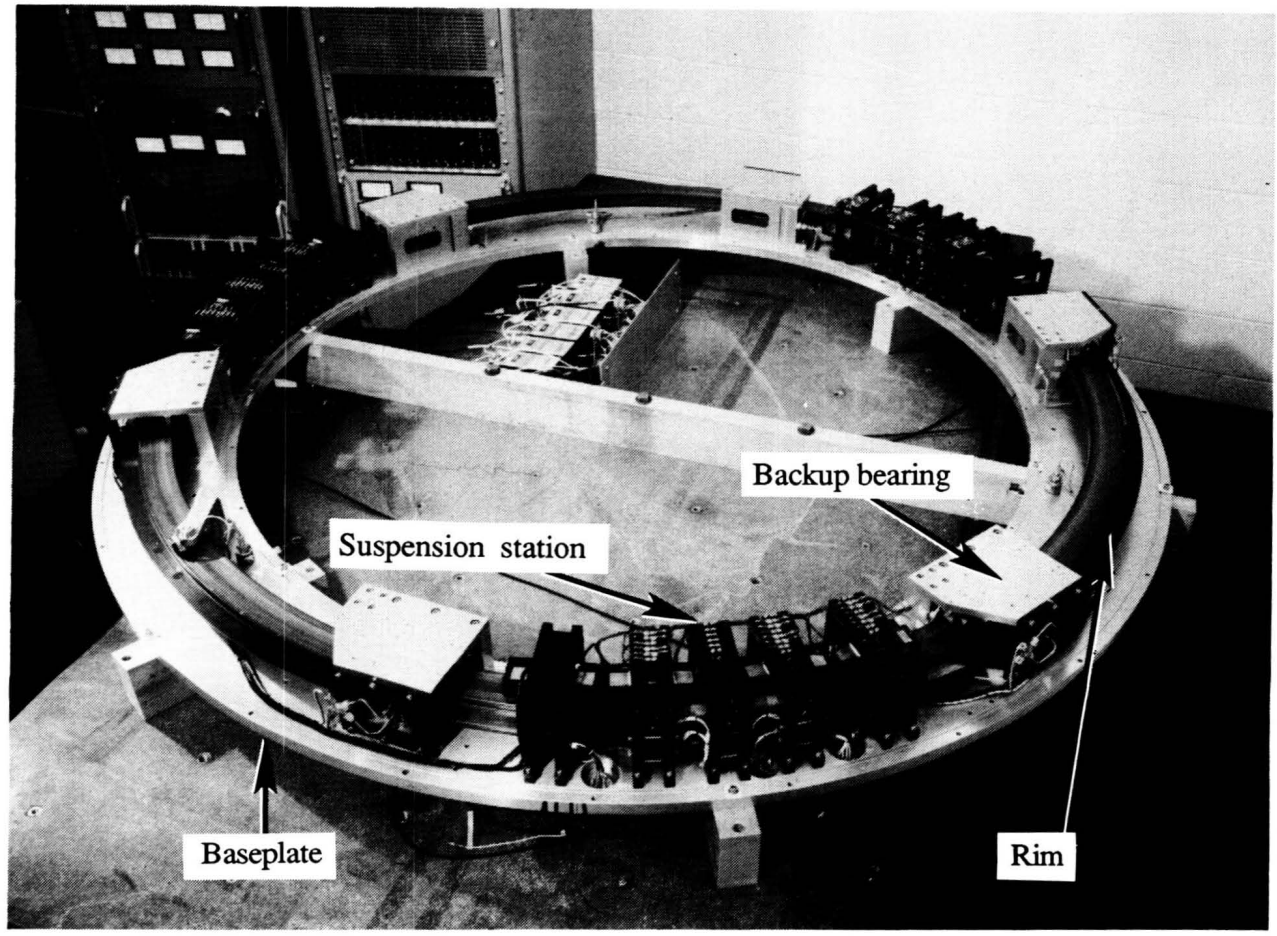

Figure 1. AMCD laboratory model.

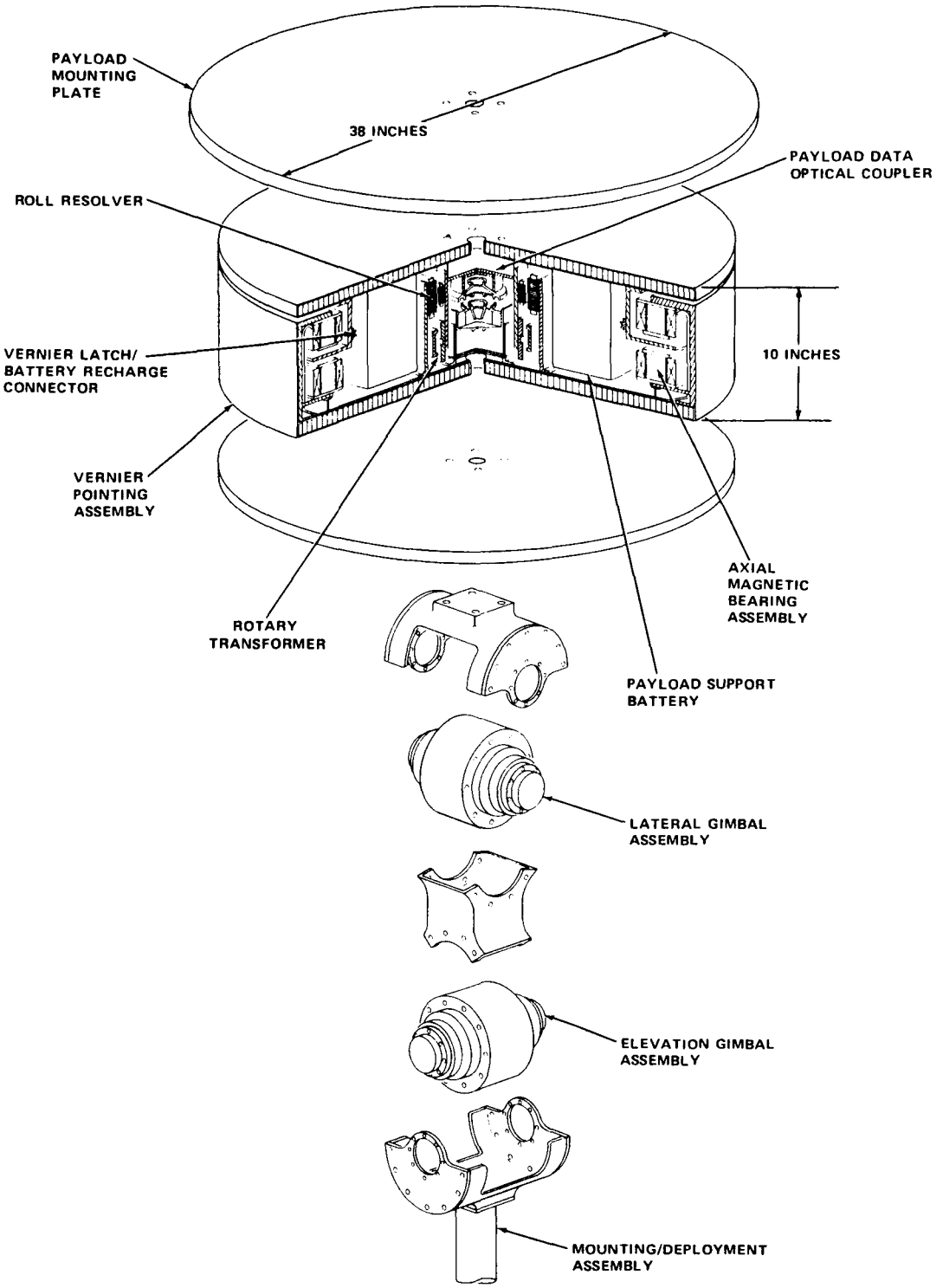

ANNULAR SUSPENSION AND POINTING SYSTEM (ASPS)–EXPLODED VIEW

Figure 2. ASPS configuration.

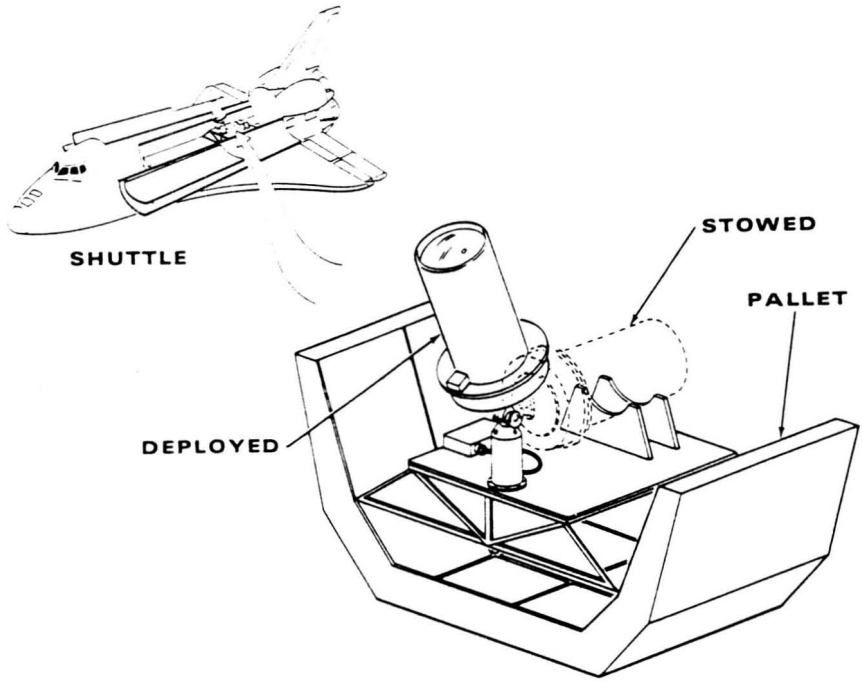

Figure 3. Typical payload ASPS carrier vehicle configuration.

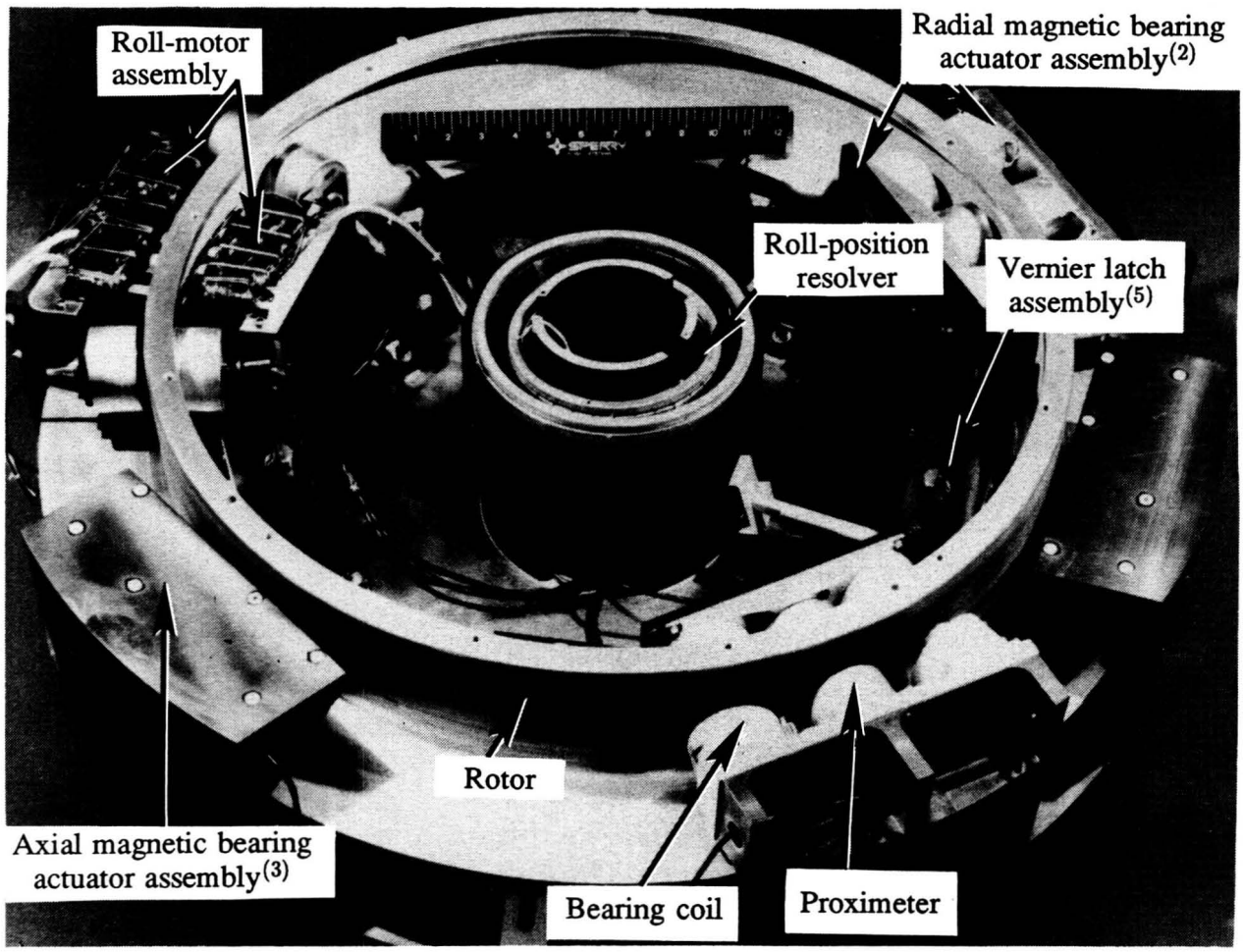

Figure 4. ASPS vernier assembly engineering model.

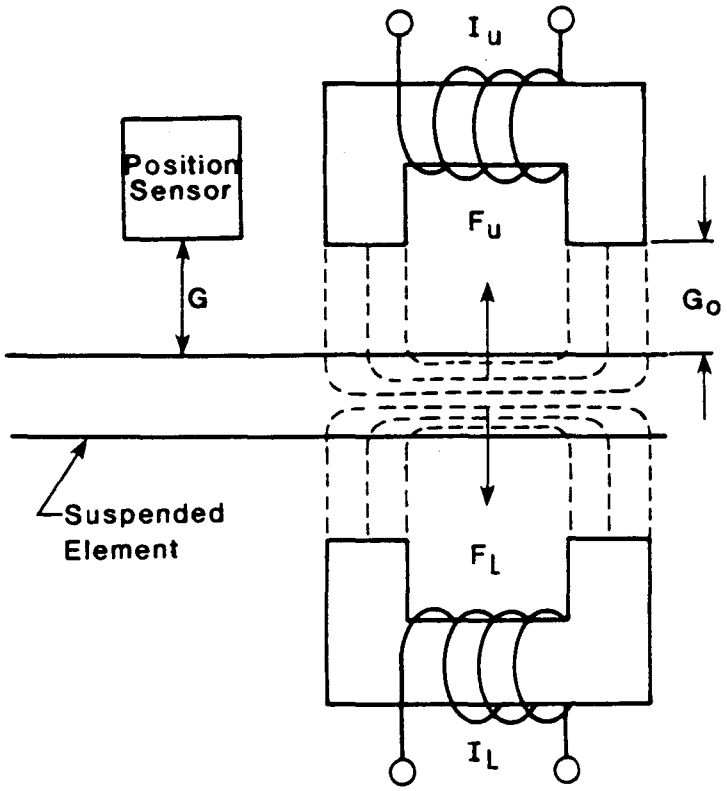

Figure 5. Magnetic bearing actuator.

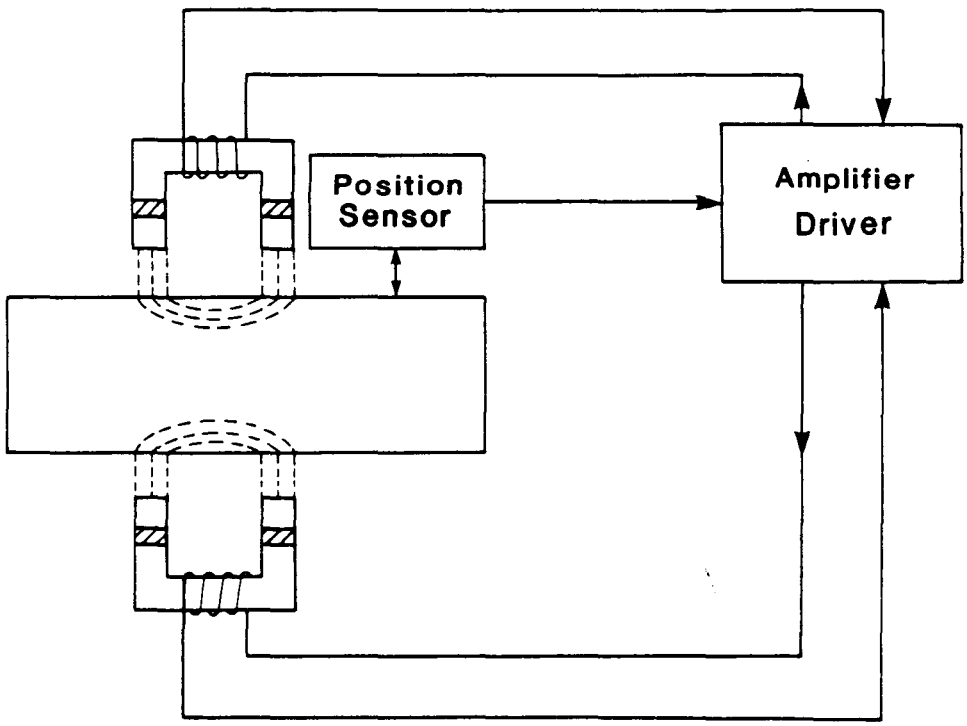

Figure 6. Permanent magnet flux-biased magnetic actuator.

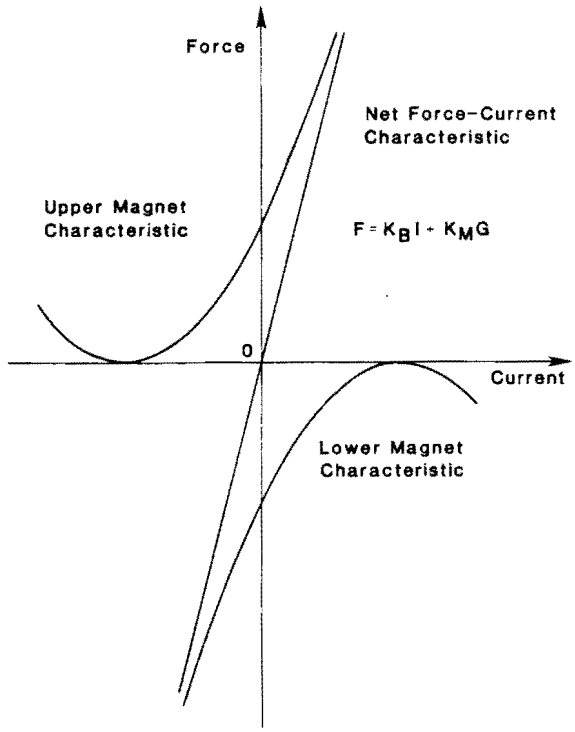

Figure 7. Force-current characteristic of a permanent magnet flux-biased magnetic actuator.

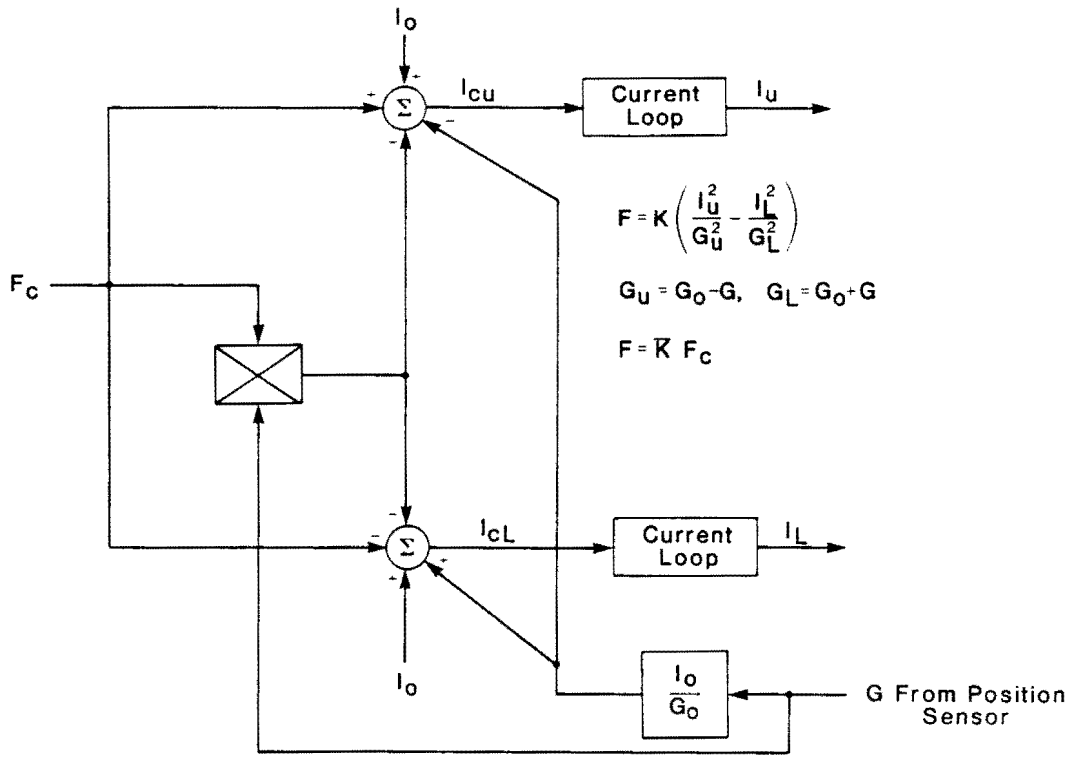

Figure 8. Variable biased current approach for magnetic actuator control.

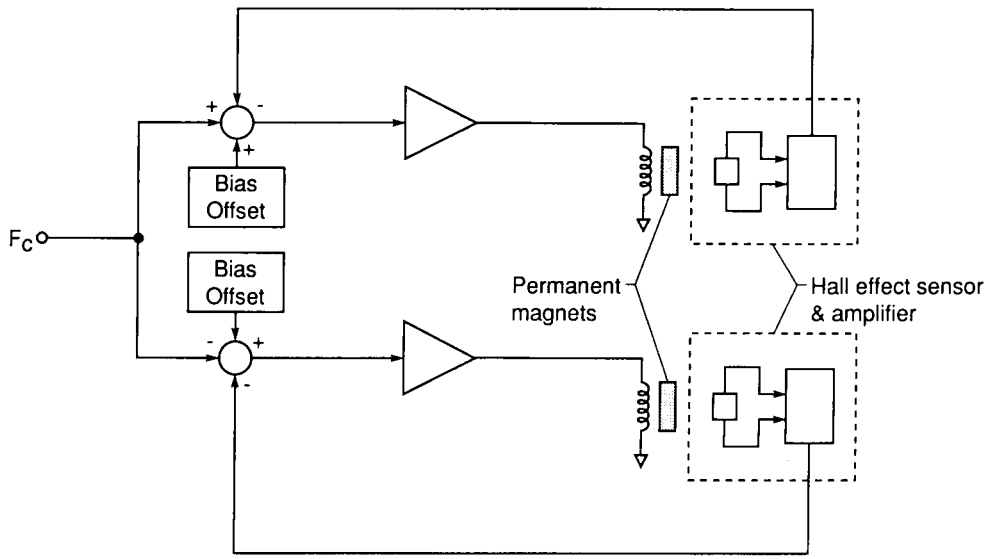

Figure 9. Flux feedback approach.

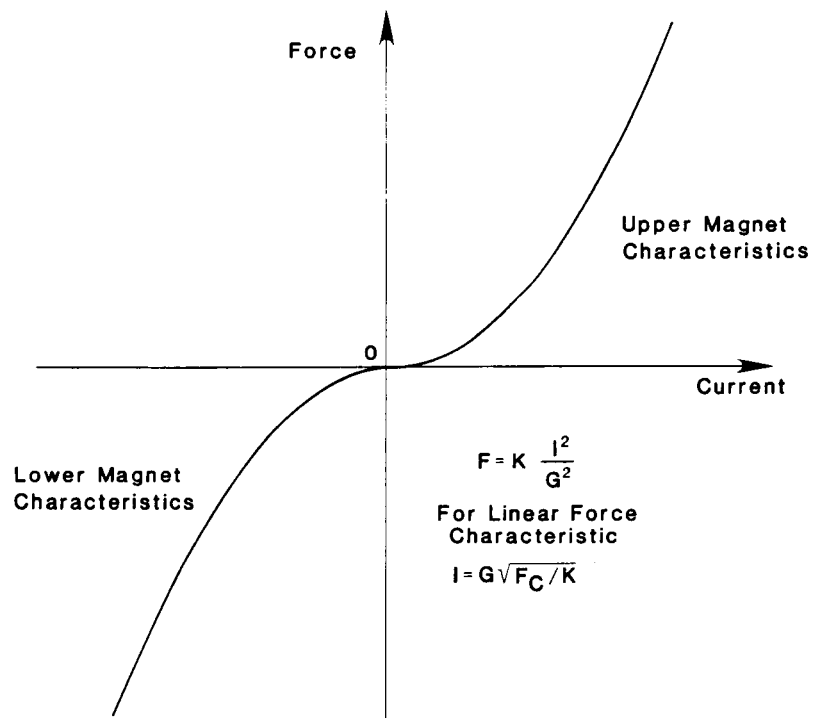

Figure 10. Force current characteristic of a magnetic actuator with individual element control.

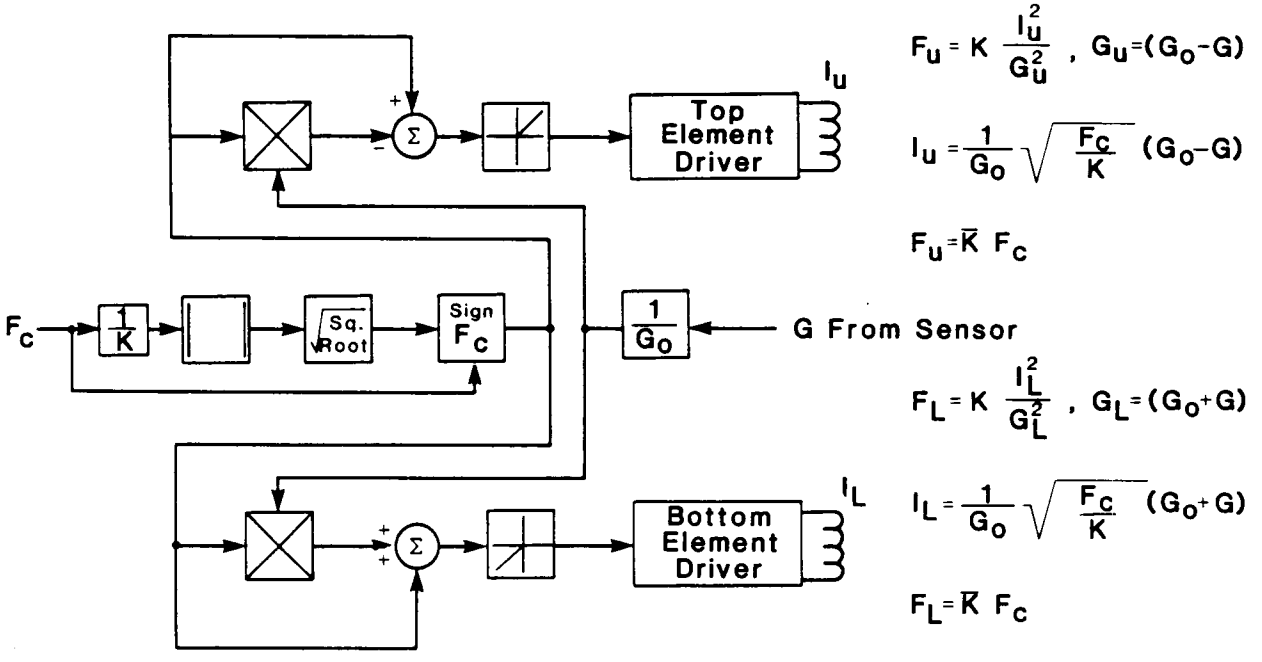

Figure 11. Analog solution of the force equation for individual element control.

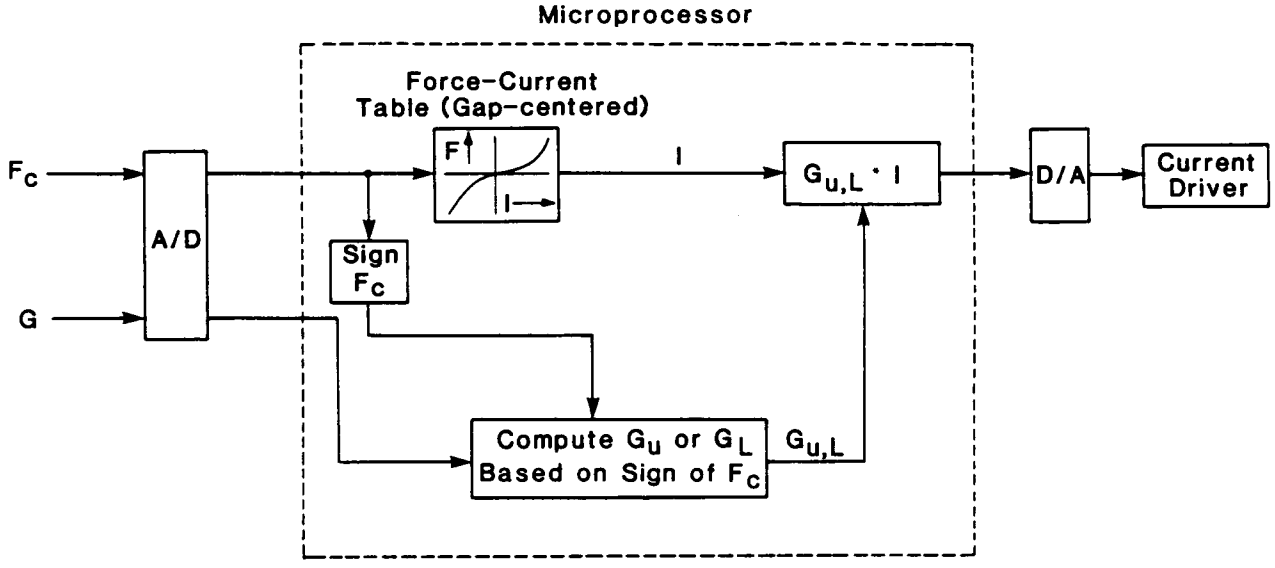

Figure 12. Table look-up approach for individual element control.

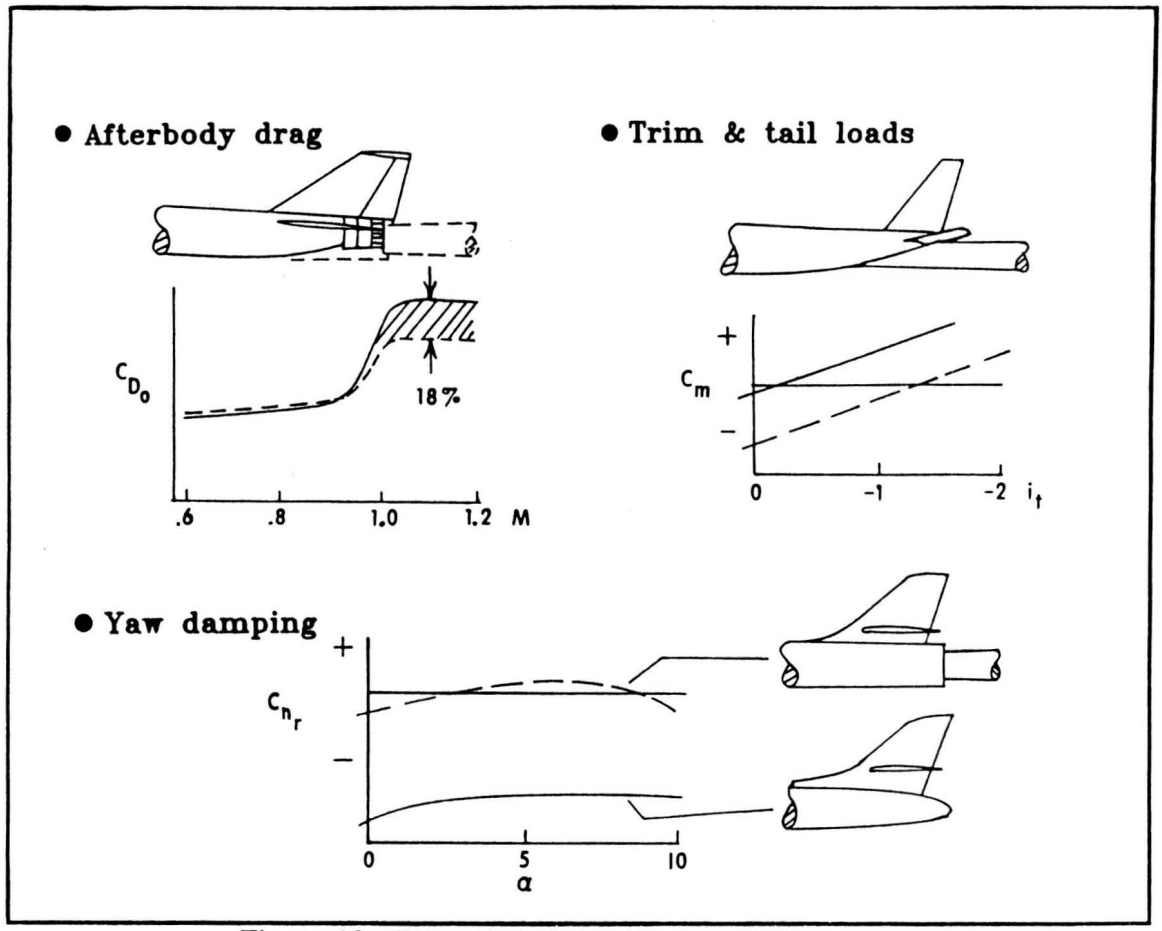

Figure 13. Examples of model support problems.

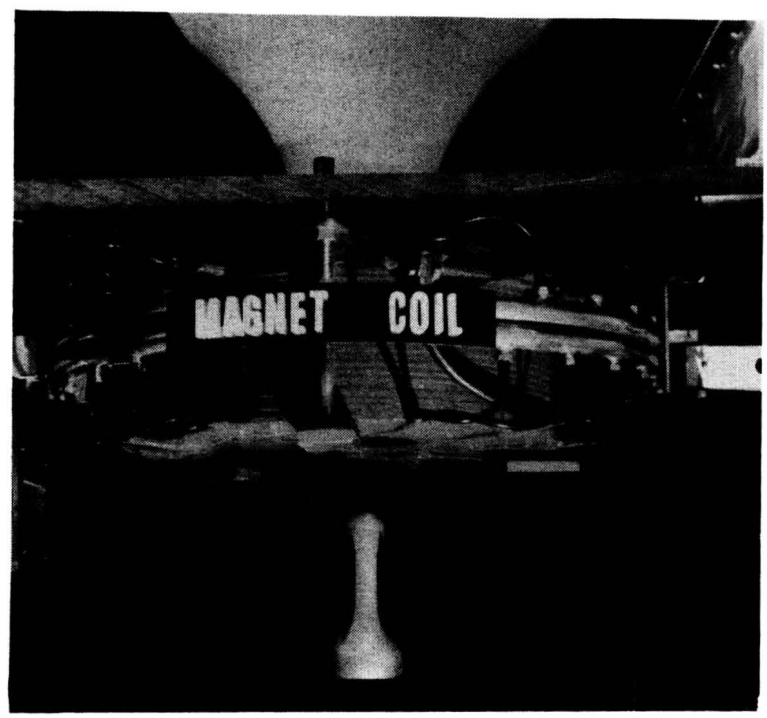

Figure 14. Photograph showing model supported in Langley magnetic suspension system.

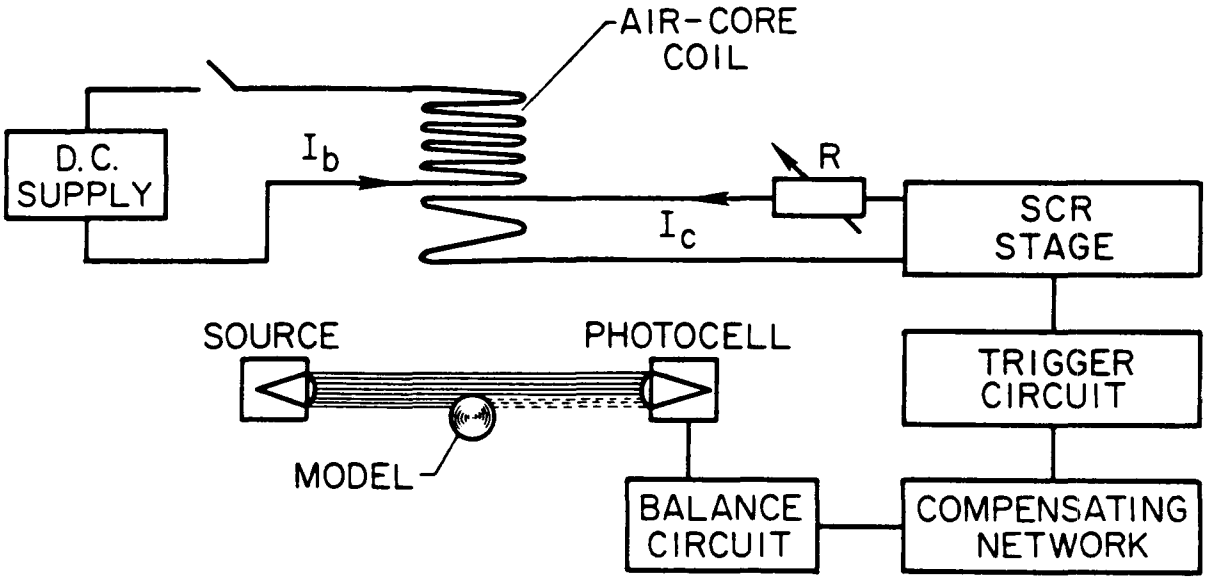

Figure 15. Schematic of major circuit components.

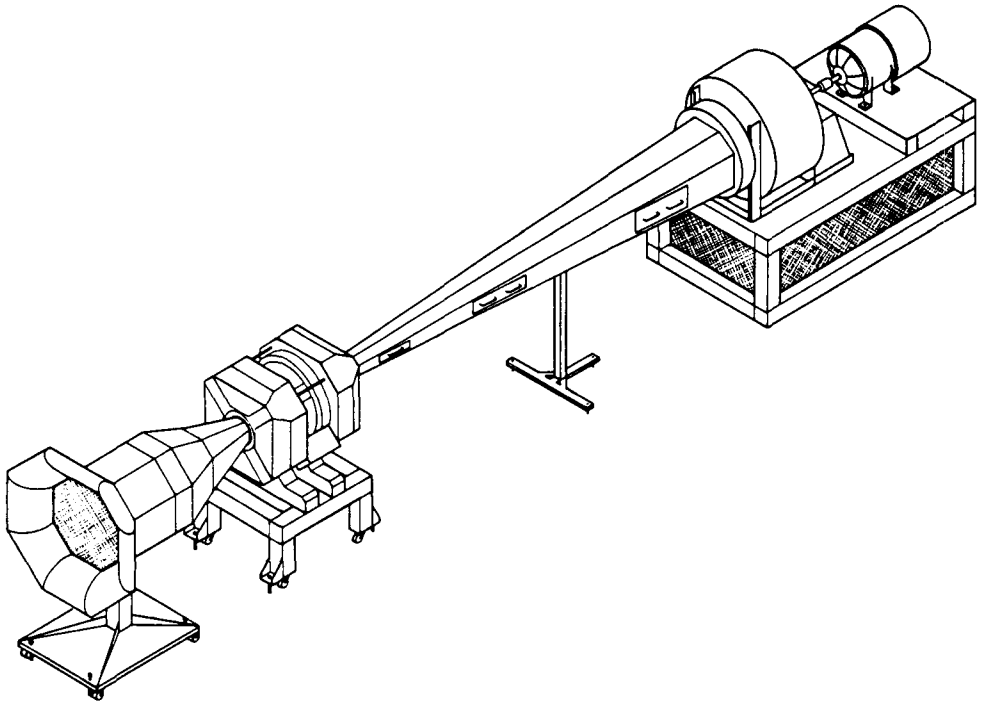

Figure 16. NASA LaRC/MIT 6-inch magnetic suspension and balance system.

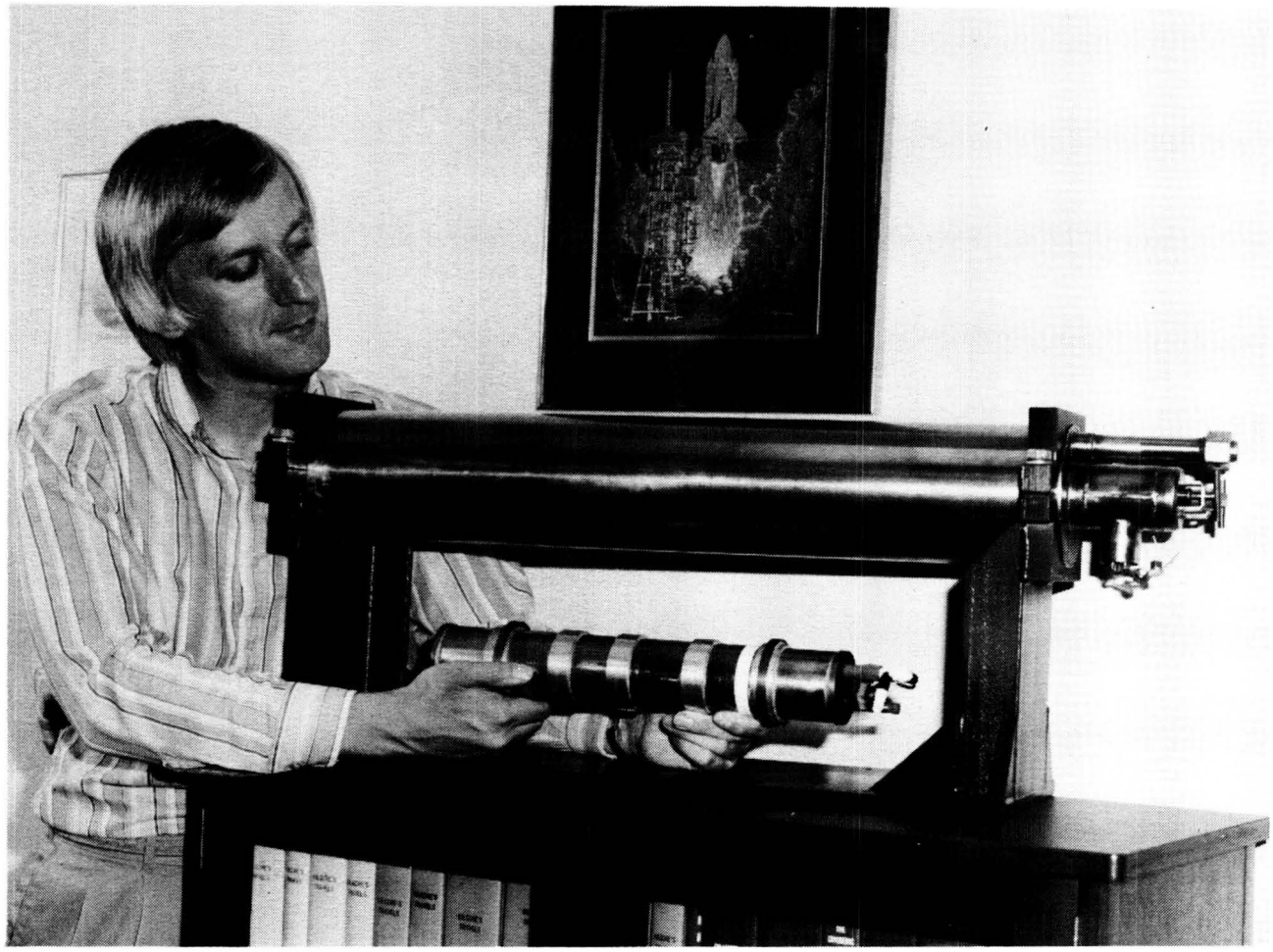

Figure 17. Superconducting solenoid.

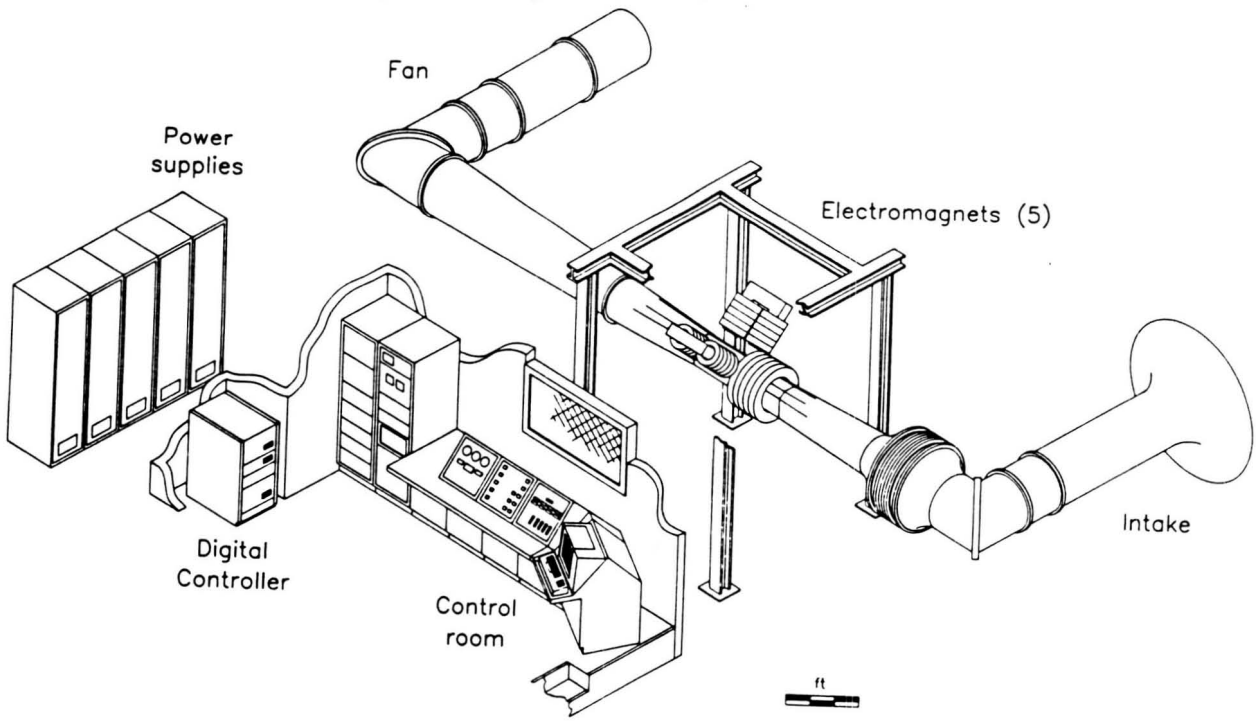

Figure 18. Thirteen inch magnetic suspension laboratory.